

Article

Synthesis, Crystal Structures, and Molecular Properties of Three Nitro-Substituted Chalcones

Alam Yair Hidalgo ¹, Manuel Velasco ¹, Eduardo Sánchez-Lara ^{2,†}, Abraham Gómez-Rivera ¹, Miguel A. Vilchis-Reyes ¹, Cuauhtémoc Alvarado ¹, Maribel Herrera-Ruiz ³, Ricardo López-Rodríguez ¹, Nancy Romero-Ceronio ^{1,*} and Carlos E. Lobato-García ¹

¹ División Académica de Ciencias Básicas, Universidad Juárez Autónoma de Tabasco, Carretera Cunduacán-Jalpa Km 1, Col. La Esperanza, Cunduacan 86690, Tabasco, Mexico; alam.yair.hidalgo@gmail.com (A.Y.H.); manuel.velasco@ujat.mx (M.V.); abraham.gomez@ujat.mx (A.G.-R.); miguel.vilchis@ujat.mx (M.A.V.-R.); cuauhtemoc.alvarado@ujat.mx (C.A.); ricardo.lopezr@ujat.mx (R.L.-R.); carlos.lobato@ujat.mx (C.E.L.-G.)

² Instituto de Ciencias, Benemérita Universidad Autónoma de Puebla, 18 Sur y Av. San Claudio, Col. San Manuel, Puebla 72570, Puebla, Mexico; esl_24@hotmail.com

³ Centro de Investigación Biomédica del Sur, Instituto Mexicano del Seguro Social, Calle Rep. Argentina #1, Xochitepec 62780, Morelos, Mexico; cibis_herj@yahoo.com.mx

* Correspondence: nancy.romero@ujat.mx

† Currently unaffiliated to Benemérita Universidad Autónoma de Puebla.



Citation: Hidalgo, A.Y.; Velasco, M.; Sánchez-Lara, E.; Gómez-Rivera, A.; Vilchis-Reyes, M.A.; Alvarado, C.; Herrera-Ruiz, M.; López-Rodríguez, R.; Romero-Ceronio, N.; Lobato-García, C.E. Synthesis, Crystal Structures, and Molecular Properties of Three Nitro-Substituted Chalcones. *Crystals* **2021**, *11*, 1589. <https://doi.org/10.3390/cryst11121589>

Academic Editor: Duncan H. Gregory

Received: 22 October 2021

Accepted: 2 December 2021

Published: 20 December 2021

Publisher's Note: MDPI stays neutral with regard to jurisdictional claims in published maps and institutional affiliations.



Copyright: © 2021 by the authors. Licensee MDPI, Basel, Switzerland. This article is an open access article distributed under the terms and conditions of the Creative Commons Attribution (CC BY) license (<https://creativecommons.org/licenses/by/4.0/>).

Abstract: Three functionalized chalcones containing combinations of nitro functional groups have been synthesized via Claisen-Schmidt condensation between 2-nitroacetophenone and nitrobenzaldehyde, and the crystal structures obtained ((*E*)-1,3-bis(2-nitrophenyl)prop-2-en-1-one, **1a**, (*E*)-1-(2-nitrophenyl)-3-(3-nitrophenyl)prop-2-en-1-one, **1b** and (*E*)-1-(2-nitrophenyl)-3-(4-nitrophenyl)prop-2-en-1-one, **1c**), C₁₅H₁₀N₂O₅, are reported. Compounds **1a** and **1c** crystallized in the triclinic centrosymmetric space group *P* $\bar{1}$, whereas compound **1b** crystallized in the orthorhombic space group *Pbca*. The X-ray analysis reveals that structures **1a** and **1b** exhibits *s-trans* conformation, whereas structure **1c** exists in *s-cis* conformation, concerning the olefinic double bonds. In addition, the results show that the position of the nitro substituent attached to the aromatic B-ring has a direct effect on the molecular coplanarity of these compounds. The Hirshfeld surface analysis suggests that the non-covalent π - π stacking interactions are the most important contributors for the crystal packing of **1a** and **1b**. In **1c**, the crystal packing is mainly stabilized by weak intermolecular C—H \cdots O interactions due to the planar nature of the molecule.

Keywords: nitro chalcone; crystal structure; Hirshfeld surface; NMR-spectroscopy

1. Introduction

Chalcones (systematic name 1,3-diphenyl-2-propen-1-one) are unique structures found in a wide range of natural and synthetic compounds and are considered one of the privileged scaffolds in the field of medicinal chemistry for drug discovery. Naturally occurring chalcones are multisubstituted in the aryl rings by different groups, mainly hydroxyl, methoxy and alkenyl functions, while their synthetic analogs contain one or more aryl substituents such as halogens, alkyl, amine-, nitro-, nitril-, acetamide-, carboxylic groups, heterocyclic, benzene and condensed rings, etc [1–4]. Among these synthetic derivatives, the nitrochalcones have generated continuous interest among chemists and biochemists, mainly because of their applications in medicinal chemistry as potential antimicrobial, anti-hyperglycemic, antinociceptive, antitumor tools [5–13]. In this sense, in a previous report, we synthesized three nitro-substituted chalcones and evaluated their anti-inflammatory activity. We found that the chalcone with the nitro group at the *ortho* position develops the strongest anti-inflammatory protective effect, whereas the chalcone with the nitro group at the *para* position, showed the smallest effect [14]. Another important aspect of

some nitro chalcones is that they can be used as intermediates for synthesizing various heterocyclic compounds like indoles, thioaurones, carbazoles, sultams, benzothiophenes, quinolines and indolin-3-ones [15–23]. On the other hand, the nitro chalcones also find application as chemosensors for anion sensing [24]. Additionally, the use of nitrochalcones as organogelators has also been reported [25].

Base on the above, it is of our interest to synthesize nitro-substituted chalcones due to their potential properties. Therefore, we herein report the synthesis, X-ray crystal structure studies and Hirshfeld surface analysis of three nitrochalcone derivatives.

2. Materials and Methods

2.1. General

All chemicals were purchased from Sigma Aldrich (Toluca, Mexico). All manipulations were carried out at room temperature with no special solvent and reagent purification. Melting points were determined on a Stuart SMP10 apparatus by the open capilar technique and are uncorrected. ^1H NMR and DEPTQ NMR spectra were recorded at 600 MHz and 150 MHz, respectively, in $\text{DMSO-}d_6$ using a Bruker AscendTM Spectrometer. Chemical shifts are given in ppm and reported to the residual solvent peak ($\text{DMSO-}d_6$: 2.50 ppm for ^1H and 39.51 ppm for ^{13}C). Data are reported as follows: chemical shift (δ), multiplicity (s = singlet, d = doublet, t = triplet, m = multiplet), coupling constant(s) (J , Hz) and integration. Analytical TLC was performed on silica gel 60 F254 plates. IR spectra were obtained using an FT-IR spectrometer, Spectrum One, Perkin Elmer.

2.2. X-ray Crystallography

Single crystals of **1a–1c**, suitable for X-ray study, were purified by a two-solvent recrystallization technique at room temperature. Data collection was performed using the Stoe Stadivari diffractometer equipped with an Axo microfocus source $\text{Ag-K}\alpha$ ($\lambda = 0.56083 \text{ \AA}$) and a Dectris Pilatus-100K detector. The absorption correction for the three compounds was realized using measurements of symmetry-related intensities (X-Area [26]). Structure solutions were obtained using direct methods implemented in SHELXS [27], and the final refinement was performed with full-matrix least-squares on F^2 using SHELXL [27]. In the case of **1c**, a positional disorder was resolved for the carbonyl atom O7, which was split over two positions, O7a and O7b, with refined occupancies 0.41(4) and 0.59(4). The programs ORTEP-3 [28] SHELXS/SHELXL [27] were used within the WinGX [28] software package. All hydrogen atoms were placed in calculated positions and refined as riding on their parent C atoms, with $\text{C—H} = 0.95 \text{ \AA}$ (**1a**) or $\text{C—H} = 0.93 \text{ \AA}$ (**1b–c**). All H atoms were refined isotropically, with $U_{\text{iso}}(\text{H}) = 1.2U_{\text{eq}}(\text{carrier C})$. Geometric parameters of **1a–1c** were validated and studied through the Mercury [29] and Platon [30] software. Crystal data, data collection and structure refinement details are summarized in Table 1. Crystallographic information files for the three chalcone derivatives were deposited in the Cambridge Structural Database [31] under codes 2036696, 2036697 and 2036695, respectively. Copies of data can be obtained free of charge at <https://www.ccdc.cam.ac.uk/> (accessed on 29 October 2021).

Table 1. Single crystal data and structure refinement details for compounds **1a**, **1b** and **1c**.

	1a	1b	1c
Empirical formula	$\text{C}_{15}\text{H}_{10}\text{N}_2\text{O}_5$	$\text{C}_{15}\text{H}_{10}\text{N}_2\text{O}_5$	$\text{C}_{15}\text{H}_{10}\text{N}_2\text{O}_5$
Formula weight	298.25	298.25	298.25
Crystal system	Triclinic	Orthorhombic	Triclinic
T (K)	123(1)	295(1)	295(1)
Space group	$P\bar{1}$	$Pbca$	$P\bar{1}$
CCDC-Numbers	2036696	2036697	2036695

Table 1. Cont.

	1a	1b	1c
Conformation	<i>s-trans</i>	<i>s-trans</i>	<i>s-cis</i>
<i>a</i> [Å]	7.6303(4)	11.1553(4)	7.6817(9)
<i>b</i> [Å]	7.8424(5)	14.1772(5)	7.8867(7)
<i>c</i> [Å]	12.5262(8)	17.6747(8)	12.4081(13)
α (deg)	94.327(5)	90	84.587(8)
β (deg)	90.696(5)	90	74.210(9)
γ (deg)	117.716(4)	90	69.877(8)
<i>V</i> (Å ³)	660.72(7)	2795.27(19)	679.20(13)
<i>Z</i>	2	8	2
Radiation type	0.56083 Å	0.56083	0.56083
θ range	2.430 to 23.000°	2.320 to 21.498°	2.553 to 21.497°
<i>D</i> _{calc.} (g/cm ³)	1.499	1.417	1.458
μ (mm ⁻¹)	0.070	0.067	0.068
Transm. factors	0.572–1.000	0.428–1.000	0.429–1.000
Reflections collected	16132	61499	14368
Independent reflections	3743	3270	3166
Parameters	199	200	209
<i>R</i> _{int}	0.0241	0.0527	0.0429
Goodness-of-fit on <i>F</i> ²	1.086	1.012	0.892
Final <i>R</i> index [<i>I</i> > 2σ(<i>I</i>)]	0.0354	0.0386	0.0424
<i>wR</i> ₂ (all data)	0.1002	0.1119	0.1199
Largest diff. peak and hole (e/Å ³)	0.341, −0.235	0.166, −0.174	0.230, −0.187

2.3. General Procedure: Synthesis of Nitro Chalcones Derivatives (1a–1c)

To a stirred solution of 2-nitroacetophenone (10 mmol) in ethanol (10 mL) was added a solution of sodium hydroxide (6 mL, 1.0 M) in an ice-salt bath. After stirring for 15 min, the appropriate nitrobenzaldehyde was added and the reaction mixture was stirred for 3 h at room temperature. The progress of the reaction was monitored by TLC. The product obtained was filtered, washed with water and recrystallized by a solvent pair (dichloromethane/*n*-hexane), which gave the desired nitro chalcone **1**.

(*E*)-1,3-bis(2-nitrophenyl)prop-2-en-1-one **1a**. Obtained in 42% yield as a white solid; mp: 140–142 °C [lit. 136–137 °C] [32]; ¹H NMR (600 MHz, DMSO-*d*₆) δ = 8.25 (d, *J* = 8.1 Hz, 1H), 8.08 (d, *J* = 8.1 Hz, 1H), 8.01 (d, *J* = 7.7 Hz, 1H), 7.95 (t, *J* = 7.3 Hz, 1H), 7.85–7.80 (m, 2H), 7.75 (d, *J* = 7.4 Hz, 1H), 7.70 (t, *J* = 7.9 Hz, 1H), 7.66 (d, *J* = 16.1 Hz, 1H), 7.24 (d, *J* = 16.1 Hz, 1H); DEPTQ NMR (150 MHz, DMSO-*d*₆) δ = 192.6, 148.8, 146.9, 141.6, 135.3, 135.1, 134.4, 132.2, 131.8, 130.0, 129.8, 129.7, 129.6, 125.3, 125.1. FTIR: ν_{\max} /cm⁻¹: 1658 (C=O), 1516 (C=C), 1333 (N—O), 977 (C=C *trans*).

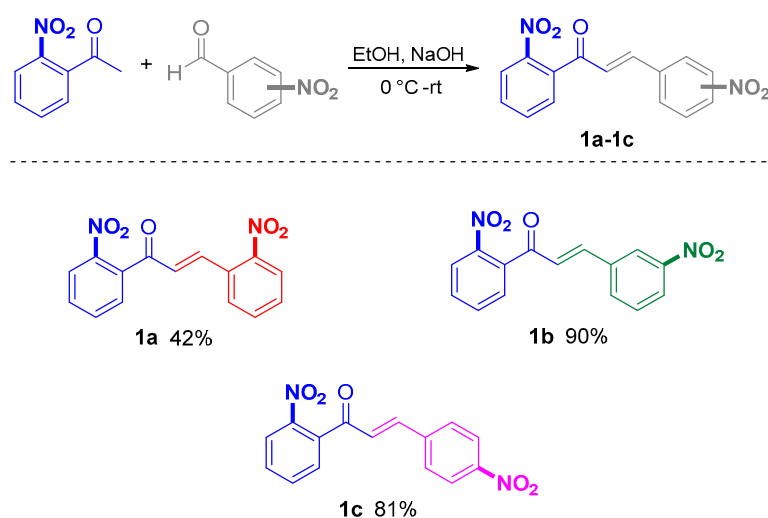
(*E*)-1-(2-nitrophenyl)-3-(3-nitrophenyl)prop-2-en-1-one **1b**. Obtained in 90% yield as a white solid; mp: 145–147 °C [lit. 143–145 °C] [32]; ¹H NMR (600 MHz, DMSO-*d*₆) δ = 8.58 (s, 1H), 8.25–8.22 (m, 3H), 7.92 (t, *J* = 7.4 Hz, 1H), 7.83 (t, *J* = 7.7 Hz, 1H), 7.74 (d, *J* = 7.4 Hz, 1H), 7.70 (t, *J* = 7.9 Hz, 1H), 7.57 (d, *J* = 16.3 Hz, 1H), 7.51 (d, *J* = 16.3 Hz, 1H); DEPTQ NMR (150 MHz, DMSO-*d*₆) δ = 192.6, 148.7, 147.0, 143.6, 136.3, 135.6, 135.0, 134.9, 132.0, 130.8, 129.5, 128.6, 125.4, 125.0, 123.9. FTIR: ν_{\max} /cm⁻¹: 1650 (C=O), 1523 (C=C), 1345 (N—O), 983 (C=C *trans*).

(*E*)-1-(2-nitrophenyl)-3-(4-nitrophenyl)prop-2-en-1-one **1c**. Obtained in 81% yield as a yellow solid; mp: 175–177 °C [lit. 168–169 °C] [32]; ¹H NMR (600 MHz, DMSO-*d*₆) δ = 8.24–8.22 (m, 3H), 8.01 (m, 2H), 7.93 (t, *J* = 7.4 Hz, 1H), 7.83 (t, *J* = 7.7 Hz, 1H), 7.76 (d, *J* = 7.4 Hz, 1H), 7.53 (d, *J* = 16.2 Hz, 1H), 7.48 (d, *J* = 16.2 Hz, 1H); DEPTQ NMR (150 MHz, DMSO-*d*₆) δ = 192.5, 148.7, 147.0, 143.1, 140.8, 135.4, 135.0, 132.1, 130.3, 129.7, 129.5, 125.1, 124.3. FTIR: ν_{\max} /cm⁻¹: 1667 (C=O), 1511 (C=C), 1334 (N—O), 983 (C=C *trans*).

3. Results and Discussion

3.1. Chemistry

The synthetic route of the proposed compound **1a–1c** is shown in Scheme 1. The nitro chalcone derivatives were obtained by the reaction of 2-nitroacetophenone with the appropriate nitrobenzaldehyde in the presence of an alcoholic basic medium [14]. All the compounds were recrystallized using a solvent pair. The yield of the compounds after recrystallization ranged from 42 to 90%. In ^1H NMR spectra, the values of the coupling constants between H_α and H_β ($J = 16.1\text{--}16.3$ Hz) confirm that, for this reaction, the products generated were only *E*-isomers. The ^1H (600 MHz) and DEPTQ (150 MHz) NMR. Spectra are presented in Supplementary Materials (Figures S1–S6). The infrared spectra of the synthesized compounds **1a–1c** exhibited similar spectral patterns (Figure S7). The IR peaks observed are consistent with the functional groups present in the compound and hence, support the structure of **1a–1c**. Table S1 shows the assignments of the main bands [33].



Scheme 1. The synthesis of compounds.

It is important to mention that the behavior observed in the melting points values for the isomers reported as **1a–c** can be described as follows: the isomers **1a** and **1b** present very similar melting points, but in the case of isomer **1c**, this physical constant is higher. We can attribute this difference in the melting points values to the fact that the latter isomer presents the flattest conformation, which allows a better packing in the crystalline lattice, thereby increasing the melting point.

3.2. Structural Description

Compound **1a** crystallized triclinic with the space group $P\bar{1}$ (Table 1). The asymmetric unit contains two nitro-substituted aromatic rings in the *ortho* position, joined by a three-carbon α,β -unsaturated carbonyl system (Figure 1). The molecule adopts the most stable *s-trans* conformation with respect to the $\text{C8}=\text{C9}$ [1.336(14) Å] and $\text{C7}=\text{O7}$ [1.217(12) Å] functional groups, located in the enone moiety [34]. The structure is twisted around the $\text{C1}'\text{—C7}$ and C9—C1 single bonds with torsion angles of $79.82(13)^\circ$ and $142.81(11)^\circ$ for $\text{C8—C7—C1}'\text{—C2}'$ and C2—C1—C9—C8 , respectively. The molecule adopts a conformation in which the —NO_2 groups are closer to each other, generating a slightly more compact asymmetric unit compared to compounds **1b** and **1c**, which have a more extended molecular backbone (see below). Therefore, this structure can be considered thermodynamically less stable compared with compounds **1b** and **1c**.

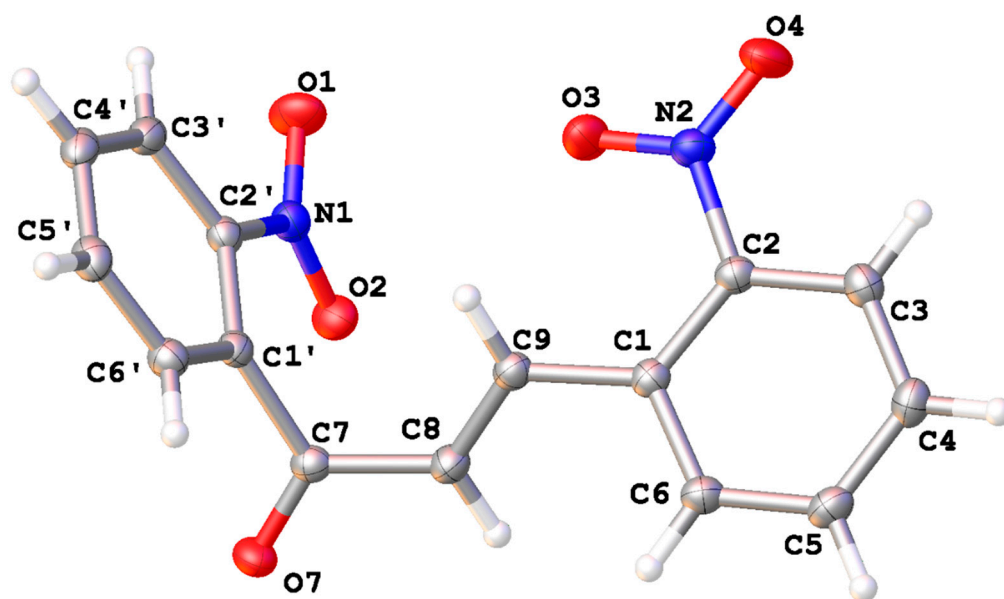


Figure 1. The molecular structure of compound **1a**, with displacement ellipsoids drawn at the 50% probability level. H atoms are shown as small spheres of arbitrary radius.

A quick analysis in *Mogul geometry check* [29] confirms the deviation of the torsion angles, C8—C7—C1'—C2' [79.82(13)°] and O7—C7—C1'—C6' [72.54(13)°], from the typical values found in chalcone derivatives. Out of 48 crystal structures analyzed from the *Mogul* library of the CSD [35], only three crystal structures (CSD refcodes: CNCHAL, BRNICH and NIPFUP) with at least one nitro-substituted aromatic ring have torsion angles similar to those of compound **1a** [36,37]. From these data, we can deduce that nitro groups have a direct effect on the degree of torsion of the molecule. This is more evident in this compound due to the electro-withdrawing groups that are in the *ortho* position in both aromatic systems [38]. As we shall see, as long as the aromatic B-ring changes its substitution pattern, the molecules assume a greater planar character. On the other hand, the two aromatic systems related by the enone group form a dihedral angle of 63.21(4)°. Finally, the nitro groups slightly deviate from the main planes of the aromatic rings with torsion angles of 13.35(14)° and −9.86(15)° for O2—N1—C2'—C1' and O3—N2—C2—C1, respectively.

Compound **1b** crystallizes orthorhombic with space group *Pbca* (Table 1). Unlike compound **1a**, the aromatic rings are nitro-substituted in *ortho* and *meta*-positions, which are connected through the —C=C—C=O planar system (Figure 2). Both NO₂-substituents are coplanar with the aromatic rings [O2—N1—C2'—C1' = −1.3(2)° and O3—N2—C3—C2 = −9.0(2)°]. The change in the substitution pattern (from *ortho*-to-*meta*) in the aromatic B-ring causes the molecule to adopt a planar moiety, and both the central enone group and the C1—C6 aromatic ring are nearly coplanar, with a torsion angle C8—C9—C1—C2 of −163.35(15)°. In contrast, the aromatic A-ring makes a torsion angle C6'—C1'—C7—C8 with the —C=C—C=O central group of 90.33(19)°. The distancing of the aromatic rings makes the nitro groups tend to be far apart from each other, minimizing the repulsive van der Waals forces. The torsion angles formed between the enone unit and the aromatic rings are also outside typical values; however, this is expected, considering the effect of the NO₂-substituent on the geometric parameters of the molecule. Compound **1b** exists in the stereoselective *s-trans* conformation with respect to the C8=C9 [1.324(2) Å] and C7=O7 [1.217(18) Å] double bonds. Apparently, this conformation is the predominant form in crystallized chalcone derivatives molecules with low planarity [39–42].

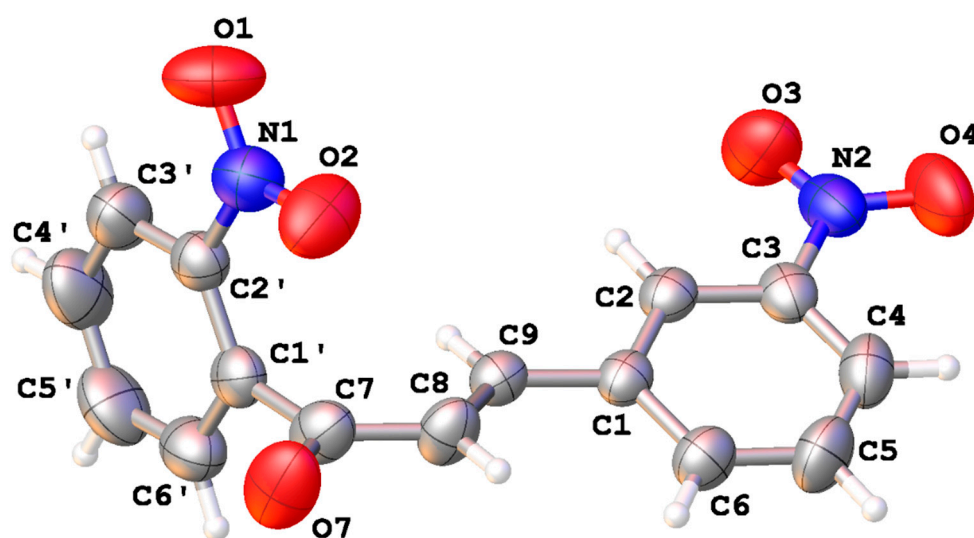


Figure 2. The molecular structure of compound **1b**, with displacement ellipsoids drawn at the 50% probability level. H atoms are shown as small spheres of arbitrary radius.

Compound **1c** crystallized triclinic with space group $P\bar{1}$ (Table 1). The geometry of the molecule is imposed by the change of position of the nitro substituent bonded to the C₄, which is in *para* position to the α, β -unsaturated carbonyl system (Figure 3). The aromatic A-ring retains the *ortho* substitution pattern in a similar way to compounds **1a** and **1b**. The torsion angles between the atoms C₈—C₉—C₁—C₆ and C₈—C₇—C₁'—C₂' are 177.6(2)° and 165.62(15)°, respectively, indicating that the substituted aromatic systems and the central enone unit are coplanar. Therefore, the molecule adopts the *s-cis* conformation with respect to the C₈=C₉ [1.321(2) Å] and C₇=O_{7B} [1.214(7) Å] double bonds, with a torsion angle C₁'—C₇—C₈—C₉ of −178.78(17)°. In contrast to compounds **1a** and **1b**, the planarity of compound **1c** favors the *s-cis* conformation, which is present in crystallized chalcone derivatives with a planar backbone [43–45].

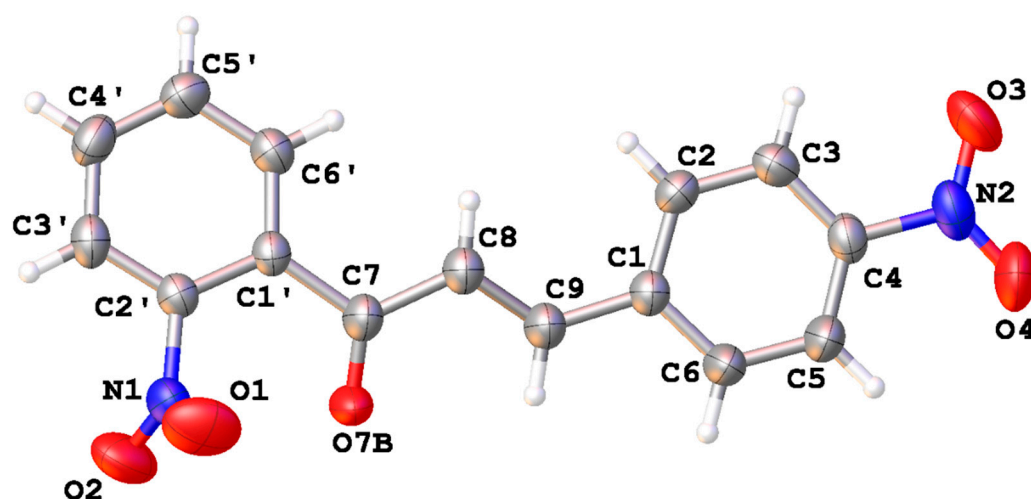


Figure 3. The molecular structure of compound **1c**, with displacement ellipsoids drawn at the 50% probability level. H atoms are shown as small spheres of arbitrary radius.

On the other hand, the dihedral angle formed between the main planes from the aromatic rings is 11.38(18)°, which is comparatively smaller than those found in **1a** and **1b**. In the molecule, the nitro substituent attached to C₄ is coplanar with the aromatic system, with a small torsion angle O₄—N₂—C₄—C₅ of 3.5(3)°, while the nitro group attached to C₂' rotates out of the aromatic plane with a torsion angle of 69.1(2)° in order to minimize electrostatic repulsions with the C₇=O_{7B} carbonyl functional group.

3.3. Supramolecular Features

Through the molecular packing diagram of compound **1a**, we can observe that both aromatic rings are involved in attractive stacking interactions with neighboring molecules placed around inversion centers from the crystallographic space group. These noncovalent interactions seem to dominate the supramolecular structure of this compound due to the lack of conventional hydrogen bonds. In this sense, the C1'—C6' aromatic rings are stacked in a parallel-displaced fashion along the [1] direction, and the separation between the centroids of this π -systems is 3.647(2) Å, while the C1—C6 aromatic rings are stacked in the same conformation with a centroid-to-centroid distance of 3.729(2) Å (Figure 4). In this scheme, the C1'—C6' aromatic ring seems to establish two short C—H \cdots O contacts with the carbonyl and nitro-group as acceptors, with intermolecular distances of 2.680(7) Å and 2.579(8) Å for C5'—H5' \cdots O7 and C4'—H4' \cdots O2, respectively, but with angles (D—H \cdots A) less than 154°.

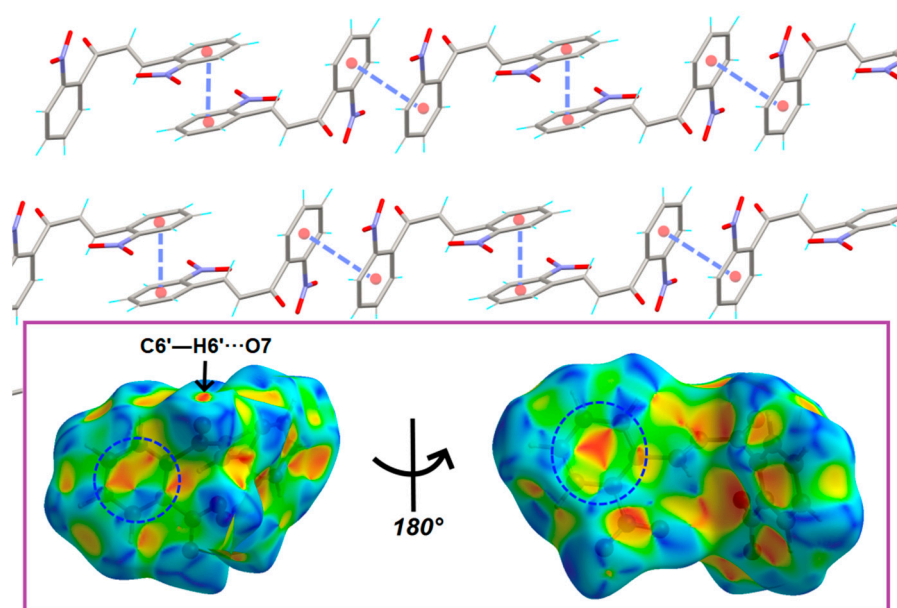


Figure 4. Part of the crystal structure of **1a**, showing the main intermolecular interactions. The inset shows the Hirshfeld surface mapped with the *shape index* property (−1.0 to 1.0 a.u) highlighting blue regions around bright-red spots within compound **1a**. The aromatic-rings involved in stacking interactions are highlighting by dashed blue circles.

It must be considered that the main supramolecular feature of **1a** is the π -stacking between the chalcone molecules; we have calculated the Hirshfeld surface with *Crystal-Explorer 17.5* [46], but instead of using the d_{norm} function (commonly used to characterize N—H \cdots O or O—H \cdots O hydrogen-bonds), we use the *shape index* property to identify planar stacking arrangements [47–49]. In a *shape index* function mapped on a Hirshfeld surface, the red hollows indicate noncovalent forces such as weak hydrogen bonds or aromatic interactions, while the blue bumps indicate spaces between neighboring molecules with little or no interaction [48].

In compound **1a** the red hollows are located on electronegative regions, which are involved in short contacts via C—H \cdots O hydrogen bonds. In other words, the C6' from aromatic ring (outside the surface) establishes a weak aromatic hydrogen-bond with O7 atom from carbonyl group as an acceptor with distance C6'—H6' \cdots O7 of 2.60(7) Å (inside the surface). This weak interaction is represented in the *shape index* as a small red depression (Figure 4). On the other hand, the pattern of blue and red triangles over both aromatic systems is strong evidence for close C \cdots C interplanar contacts, while the green and yellow regions surrounding the aromatic rings are caused by the symmetrical effect of the nitro-

groups (Figure 4, inset). The C...C stacking interactions represent 6.2% of the all interactions contained in the crystal according to the 2D-fingerprint plot (Figure S11) [50,51].

In the crystal of compound **1b**, the molecules also are held together via short C—H...O contacts, where the O atoms from carbonyl and nitro groups serve as acceptor groups. In a similar way to compound **1a**, the π -stacking interactions seem to dominate the crystal packing. The molecules are packing in dimers, favoring the interaction between the planar moieties. In this way, the C1—C6 aromatic rings are stacked in a parallel-displaced fashion with a distance of 3.862(13) Å between the centroids of two inversion-related aromatic rings (Figure 5). The blue and red triangular region on the C1—C6 aromatic ring in the *shape index* surface confirms the C...C stacking interactions between these systems (Figure 5, inset). The supramolecular assembly is additionally supported by weak C—H... π interactions, implicating the phenyl rings. According to the *shape index* property, these contacts are observed as a large red depression caused by the proximity of the C1'—C6' aromatic ring to the C1—C6 system.

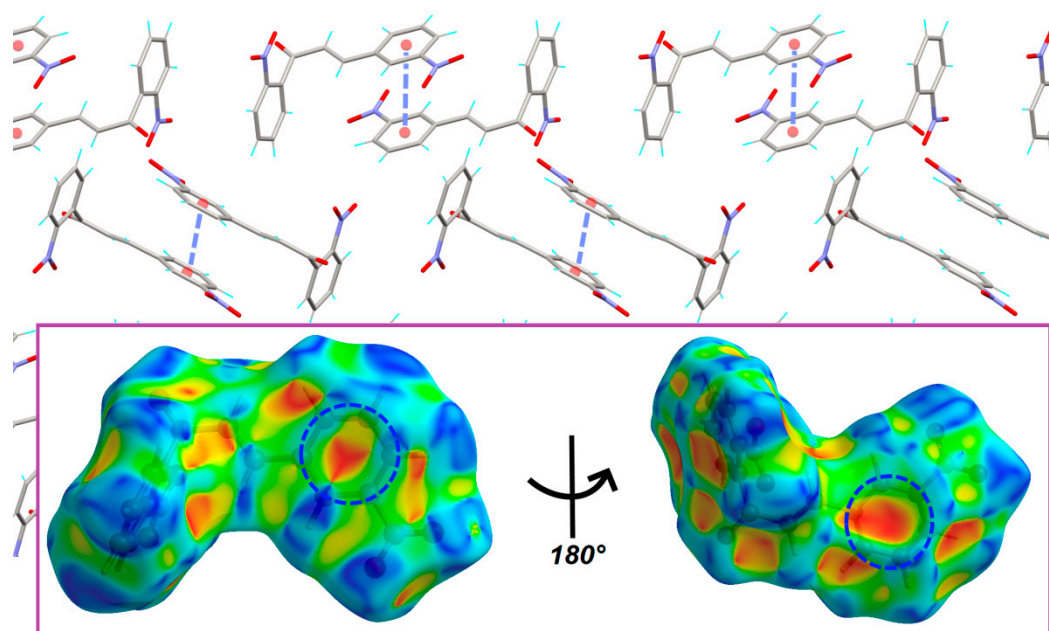


Figure 5. Part of the crystal structure of **1b**, showing intermolecular interactions between the molecules. The inset shows the Hirshfeld surface mapped with the shape index property (−1.0 to 1.0 a.u.), highlighting blue regions around bright-red spots within compound **1b**. The aromatic-rings involved in aromatic interactions are highlighting by dashed blue circles.

Due to the planar geometry of compound **1c**, the crystal structure is characterized by a sheet-like alignment of molecules running parallel to the [101] direction. Each layer is formed by inversion-related molecules interacting through C—H...O short contacts, forming $R_2^2(16)$ and $R_4^4(20)$ graph-set motifs according to Etter's nomenclature (Figure 6) [52,53]. These infinite layers are stacked on each other, showing additional intermolecular π - π stacking interactions between the C1'—C6' aromatic rings with a centroid-to-centroid distance of 3.80(4) Å, stabilizing the crystal packing in direction of the crystallographic *a*-axis. The Hirshfeld surface mapped over d_{norm} shows red spots where the contacts are shorter than vdW separations [48–54]. Regarding compound **1c**, these spots are related to regions occupied by the nitro and carbonyl groups, which are involved in weak C—H...O hydrogen bonds with neighboring molecules (see inset, Figure 6). These noncovalent interactions represent ca. 50% of all interactions in the crystal, considering reciprocal contacts, according to the 2D fingerprint plot (Figure S12).

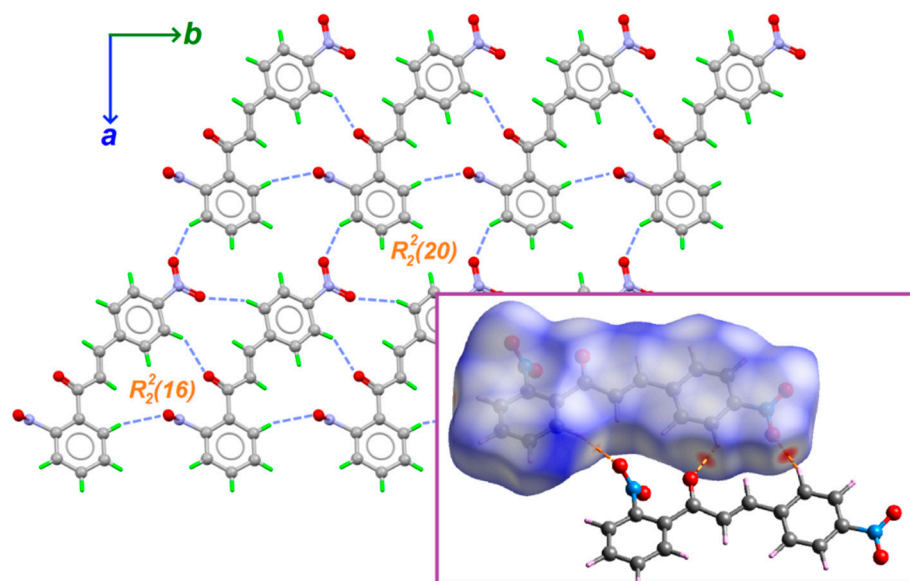


Figure 6. View of the 2D layer structure of **1c** in the *ab* plane. The inset displays the Hirshfeld surface mapped on d_{norm} property (-0.22 to 1.27 Å), where the orange dashed lines show the contacts of C—H...O with a neighboring chalcone molecule.

4. Conclusions

In summary, we have successfully prepared chalcones containing the —NO₂ group. Crystal structures show that **1a** and **1b** exhibit *s-trans* conformation, while **1c** isomer crystallized in the *s-cis* conformation. Varying the position of the nitro group on the aromatic B-ring produces a direct effect on the molecular coplanarity and consequently, on the crystal packing. The chalcone **1c** with the nitro group at the *para* position showed better molecular coplanarity between aromatic rings and the enone moiety. Intermolecular close contacts in the crystal structures of **1a–1c** by Hirshfeld surface analysis were visualized and quantified. Intermolecular π -stacking (in **1a–1b**) and C—H...O (in **1c**) interactions are the most important contributors to the crystal packing.

Supplementary Materials: The following are available online at <https://www.mdpi.com/article/10.3390/cryst11121589/s1>, Figure S1: ¹H NMR (600 MHz, DMSO-d₆) of compound **1a**, Figure S2: DEPTQ NMR (150 MHz, DMSO-d₆) of compound **1a**, Figure S3: ¹H NMR (600 MHz, DMSO-d₆) of compound **1b**, Figure S4: DEPTQ NMR (150 MHz, DMSO-d₆) of compound **1b**, Figure S5: ¹H NMR (600 MHz, DMSO-d₆) of compound **1c**, Figure S6: DEPTQ NMR (150 MHz, DMSO-d₆) of compound **1c**, Figure S7: FT-IR Spectrum of **1a–1c**, Figure S8: A view of the crystal packing down the *b* axis for compound **1a**, Figure S9: A view of the crystal packing down the *b* axis for compound **1b**, Figure S10: A view of the crystal packing down a axis for compound **1c**, Figure S11: The two-dimensional fingerprint plot of **1a**, Figure S12: The two-dimensional fingerprint plot of **1c**, Table S1: Assignment of characteristic vibrational frequencies for **1a–1c**, Table S2: Selected Bond lengths [Å] and angles [°] for **1a**, Table S3: Selected Bond lengths [Å] and angles [°] for **1b**, Table S4: Selected Bond lengths [Å] and angles [°] for **1c**, Table S5: Hydrogen-bond for **1a**, Table S6: Hydrogen-bond for **1b**, Table S7: Hydrogen -bonds for **1c**.

Author Contributions: Conceptualization and methodology: N.R.-C., M.A.V.-R. and A.Y.H.; Software and validation: E.S.-L. and C.A.; Formal analysis, investigation, resources: A.Y.H., A.G.-R., R.L.-R. and M.H.-R. Data curation writing-original: A.Y.H., E.S.-L. and M.V. Draft preparation, and writing-review and editing: C.E.L.-G., N.R.-C., A.G.-R. and R.L.-R., Visualization: M.V. and C.A.; Supervision, project administration and funding acquisition: A.G.-R., C.E.L.-G., M.A.V.-R., C.A. and N.R.-C. All authors have read and agreed to the published version of the manuscript.

Funding: The authors are grateful to PRODEP and CONACyT by financial support provided for this research by the projects: UJAT-EXB-242, CONACyT-226155 and CONACyT-268178.

Institutional Review Board Statement: Not applicable.

Informed Consent Statement: Not applicable.

Data Availability Statement: All data have been included in Supplementary Materials.

Acknowledgments: A.Y.H. wish to thank CONACyT (Mexico) for the fellowship support number 861538. M.V. was supported by PRODEP postdoctoral fellowship (14812). R.L.-R. (478597) was supported by CONACyT postdoctoral fellowship (866998). The authors acknowledge Sylvain Bernès for carrying out the X-ray diffraction experiment performed on a Stoe Stadivari diffractometer, and for the refinement process of the reported crystal structures.

Conflicts of Interest: The authors declare no conflict of interest.

References

1. Zhuang, C.; Zhang, W.; Sheng, C.; Zhang, W.; Xing, C.; Miao, Z. Chalcone: A privileged structure in medicinal chemistry. *Chem. Rev.* **2017**, *117*, 7762–7810. [[CrossRef](#)]
2. Rammohan, A.; Reddy, J.S.; Sravya, G.; Rao, C.N.; Zyryanov, G.V. Chalcone synthesis, properties and medicinal applications: A review. *Environ. Chem. Lett.* **2020**, *18*, 433–458. [[CrossRef](#)]
3. Rozmer, Z.; Perjési, P. Naturally occurring chalcones and their biological activities. *Phytochem. Rev.* **2016**, *15*, 87–120. [[CrossRef](#)]
4. Rivière, C. Dihydrochalcones: Occurrence in the plant kingdom, chemistry and biological activities. In *Studies in Natural Products Chemistry*; Atta-ur-Rahman, Ed.; Elsevier: Amsterdam, The Netherlands, 2016; Volume 51, Chapter 7; pp. 253–381.
5. Sharma, V.; Singh, G.; Kaur, H.; Saxena, A.K.; Ishar, M.P.S. Synthesis of β -ionone derived chalcones as potent antimicrobial agents. *Bioorg. Med. Chem. Lett.* **2012**, *22*, 6343–6346. [[CrossRef](#)] [[PubMed](#)]
6. Bondock, S.; Naser, T.; Ammar, Y.-A. Synthesis of some new 2-(3-pyridyl)-4,5-disubstituted thiazoles as potent antimicrobial agents. *Eur. J. Med. Chem.* **2013**, *62*, 270–279. [[CrossRef](#)]
7. Damazio, R.G.; Zanatta, A.P.; Cazarolli, L.H.; Mascarello, A.; Chiaradia, L.D.; Nunes, R.J.; Yunes, R.A.; Silva, F.R.M.B. Nitrochalcones: Potential in vivo insulin secretagogues. *Biochimie* **2009**, *91*, 1493–1498. [[CrossRef](#)]
8. Tajammal, A.; Batool, M.; Ramzan, A.; Samra, M.M.; Mahnoor, I.; Verpoort, F.; Irfan, A.; Al-Sehemi, A.G.; Munawar, M.A.; Basra, M.A.R. Synthesis, antihyperglycemic activity and computational studies of antioxidant chalcones and flavanones derived from 2, 5 dihydroxyacetophenone. *J. Mol. Struct.* **2017**, *1148*, 512–520. [[CrossRef](#)]
9. Higgs, J.; Wasowski, C.; Marcos, A.; Jukič, M.; Paván, C.H.; Gobec, S.; de Tezanos Pinto, F.; Coletti, N.; Marder, M. Chalcone derivatives: Synthesis, in vitro and in vivo evaluation of their anti-anxiety, anti-depression and analgesic effects. *Heliyon* **2019**, *5*, e01376. [[CrossRef](#)]
10. Zhang, B.; Duan, D.; Ge, C.; Yao, J.; Liu, Y.; Li, X.; Fang, J. Synthesis of xanthohumol analogues and discovery of potent thioredoxin reductase inhibitor as potential anticancer agent. *J. Med. Chem.* **2015**, *58*, 1795–1805. [[CrossRef](#)]
11. Mai, C.W.; Yaeghoobi, M.; Abd-Rahman, N.; Kang, Y.B.; Pichika, M.R. Chalcones with electron-withdrawing and electron-donating substituents: Anticancer activity against TRAIL resistant cancer cells, structure-activity relationship analysis and regulation of apoptotic proteins. *Eur. J. Med. Chem.* **2014**, *77*, 378–387. [[CrossRef](#)]
12. Jardim, G.A.M.; Guimarães, T.T.; Pinto, M.C.F.R.; Cavalcanti, B.C.; de Farias, K.M.; Pessoa, C.; Gatto, C.C.; Nair, D.K.; Namboothiri, I.N.N.; da Silva Júnior, E.N. Naphthoquinone-based chalcone hybrids and derivatives: Synthesis and potent activity against cancer cell lines. *Med. Chem. Commun.* **2015**, *6*, 120–130. [[CrossRef](#)]
13. Bandeira, P.N.; Lemos, T.L.G.; Santos, H.S.; Carvalho, M.C.S.; Pinheiro, D.P.; Morais-Filho, M.O.; Pessoa, C.; Barros-Nepomuceno, F.W.A.; Rodrigues, T.H.; Ribeiro, P.R.V.; et al. Synthesis, structural characterization, and cytotoxic evaluation of chalcone derivatives. *Med. Chem. Res.* **2019**, *28*, 2037. [[CrossRef](#)]
14. Gómez-Rivera, A.; Aguilar-Mariscal, H.; Romero-Ceronio, N.; Roa-de la Fuente, L.F.; Lobato-Garcia, C.E. Synthesis and anti-inflammatory activity of three nitro chalcones. *Bioorg. Med. Chem. Lett.* **2013**, *23*, 5519–5522. [[CrossRef](#)]
15. Zhang, G.; Lin, L.; Yang, K.; Wang, S.; Feng, Q.; Zhu, J.; Song, Q. 3-Aminoindole Synthesis from 2-Nitrochalcones and Ammonia or Primary Amines. *Adv. Synth. Catal.* **2019**, *361*, 3718–3722. [[CrossRef](#)]
16. Nguyen, T.B.; Retailleau, P. Cooperative Activating Effect of Tertiary Amine-DMSO on Elemental Sulfur: Direct Access to Thioaurones from 2'-Nitrochalcones under Mild Conditions. *Org. Lett.* **2018**, *20*, 186–189. [[CrossRef](#)]
17. Poudel, T.N.; Lee, Y.R. Construction of highly functionalized carbazoles via condensation of an enolate to a nitro group. *Chem. Sci.* **2015**, *6*, 7028–7033. [[CrossRef](#)]
18. González, J.F.; Rocchi, D.; Tejero, T.; Merino, P.; Menéndez, J.C. One-Pot Synthesis of Functionalized Carbazoles via a CAN-Catalyzed Multicomponent Process Comprising a C—H Activation Step. *J. Org. Chem.* **2017**, *82*, 7492–7502. [[CrossRef](#)] [[PubMed](#)]
19. Nguyen, T.B.; Retailleau, P. Redox-Neutral Access to Sultams from 2-Nitrochalcones and Sulfur with Complete Atom Economy. *Org. Lett.* **2017**, *19*, 3879–3882. [[CrossRef](#)]
20. Nguyen, T.B.; Retailleau, P. DIPEA-Promoted Reaction of 2-Nitrochalcones with Elemental Sulfur: An Unusual Approach to 2-Benzoylbenzothiophenes. *Org. Lett.* **2017**, *19*, 4858–4860. [[CrossRef](#)]
21. Umeda, R.; Kouno, H.; Kitagawa, T.; Okamoto, T.; Kawashima, K.; Mashino, T.; Nishiyama, Y. Selective Synthesis of Quinolines and Indoles: Sulfur-Assisted or Selenium-Catalyzed Reaction of β -(2-Nitrophenyl)- α,β -Unsaturated Ketones with Carbon Monoxide. *Heteroat. Chem.* **2014**, *25*, 698–703. [[CrossRef](#)]

22. Lin, Z.; Hu, Z.; Zhang, X.; Dong, J.; Liu, J.-B.; Chen, D.-Z.; Xu, X. Tandem Synthesis of Pyrrolo[2,3-b]quinolones via Cadogen-Type Reaction. *Org. Lett.* **2017**, *19*, 5284–5287. [[CrossRef](#)]
23. Aksenov, N.A.; Aksenov, D.A.; Arutiunov, N.A.; Aksenova, D.S.; Aksenov, A.V.; Rubin, M. Unexpected Cyclization of ortho-nitrochalcones into 2-Alkylideneindolin-3-ones. *RSC Adv.* **2020**, *10*, 18440–18450. [[CrossRef](#)]
24. Shan, Y.; Liu, Z.; Cao, D.; Sun, Y.; Wang, K.; Chen, H. Nitro substituted chalcone derivatives as quick-response chemosensors for cyanide anions. *Sens. Actuators B Chem.* **2014**, *198*, 15–19. [[CrossRef](#)]
25. Simon, F.-X.; Nguyen, T.-T.-T.; Schmutz, M.; Decher, G.; Nicoud, J.-F.; Mésini, P.J. Nitrochalcones as organogelators: Evidence of the involvement of nitro groups and solvent in gel formation. *New J. Chem.* **2009**, *33*, 2028–2033. [[CrossRef](#)]
26. Stoe & Cie. X-AREA and X-RED32; Stoe & Cie: Darmstadt, Germany, 2009.
27. Sheldrick, G.M. Crystal structure refinement with SHELXL. *Acta Crystallogr. Sect. C Struct. Chem.* **2015**, *71*, 3–8. [[CrossRef](#)]
28. Farrugia, L.J. WinGX and ORTEP for Windows: An update. *J. Appl. Crystallogr.* **2012**, *45*, 849–854. [[CrossRef](#)]
29. Macrae, C.F.; Sovago, I.; Cottrell, S.J.; Galek, P.T.A.; McCabe, P.; Pidcock, E.; Platings, M.; Shields, G.P.; Stevens, J.S.; Towler, M.; et al. Mercury 4.0: From visualization to analysis, design and prediction. *J. Appl. Crystallogr.* **2020**, *53*, 226–235. [[CrossRef](#)] [[PubMed](#)]
30. Spek, A.L. Single-crystal structure validation with the program PLATON. *J. Appl. Crystallogr.* **2003**, *36*, 7–13. [[CrossRef](#)]
31. Groom, C.R.; Allen, F.H. The Cambridge Structural Database in retrospect and prospect. *Angew. Chem. Int. Ed.* **2014**, *53*, 662–671. [[CrossRef](#)] [[PubMed](#)]
32. Kinkle, P.; Gibian, H. Uber Chalkone. *Chem. Ber.* **1961**, *94*, 26–38.
33. Prabhu, S.R.; Jayarama, A.; Chandrasekharan, K.; Upadhyaya, V. Synthesis, growth, structural characterization, Hirshfeld analysis and nonlinear optical studies of a methyl substituted chalcone. *J. Mol. Struct.* **2007**, *1136*, 244–252. [[CrossRef](#)]
34. Gomes, M.N.; Muratov, E.N.; Pereira, M.; Peixoto, J.C.; Rosseto, L.P.; Cravo, P.V.L.; Andrade, C.H.; Neves, B.J. Chalcone derivatives: Promising starting points for drug design. *Molecules* **2017**, *22*, 1210. [[CrossRef](#)] [[PubMed](#)]
35. Bruno, I.J.; Cole, J.C.; Kessler, M.; Luo, J.; Sam Motherwell, W.D.; Parkis, L.H.; Smith, B.R.; Taylor, R.; Copper, R.I.; Harris, S.E.; et al. Retrieval of Crystallographic-Derived Molecular Geometry Information. *J. Chem. Inf. Comput. Sci.* **2004**, *44*, 2133–2144. [[CrossRef](#)] [[PubMed](#)]
36. Jungk, A.E.; Schmidt, G.M.J. Conformational studies. Part II. Crystal and molecular structures of 3-bromo-, 3-chloro-, and 4-bromo-2'-nitrochalcone. *J. Chem. Soc. B Phys. Org.* **1970**, 1427–1434. [[CrossRef](#)]
37. Carpy, A.; Leger, J.M.; Nuhrich, A. 1-(2-nitrophenyl)-3-(5-nitro-2-furyl)-2-propen-1-one, C₁₃H₈N₂O₆. *Cryst. Struct. Commun.* **1978**, *7*, 361–364.
38. Jezuita, A.; Ejsmont, K.; Szatyłowicz, H. Substituent effects of nitro group in cyclic compounds. *Struct. Chem.* **2021**, *32*, 179–203. [[CrossRef](#)]
39. Hussein, H.A.; Fadhil, G.F. Theoretical investigation of para amino-dichloro chalcone isomers, part I: A DFT structure—stability study. *J. Phys. Org. Chem.* **2020**, *33*, e4073. [[CrossRef](#)]
40. Zainuri, D.A.; Razak, I.A.; Arshad, S. Molecular structure, DFT studies and UV-Vis absorption of two new linear fused ring chalcones: (E)-1-(anthracen-9-yl)-3-(2-methoxyphenyl) prop-2-en-1-one and (E)-1-(anthracen-9-yl)-3-(3-fluoro-4-methoxyphenyl) prop-2-en-1-one. *Acta Crystallogr. Sec. E Crystallog. Commun.* **2018**, *74*, 1087–1092. [[CrossRef](#)]
41. Ramos, R.R.; da Silva, C.C.; Guimarães, F.F.; Martins, F.T. Polymorphism and conformerism in chalcones. *CrystEngComm* **2016**, *18*, 2144–2154. [[CrossRef](#)]
42. Yu, F.; Wang, M.; Sun, H.; Shan, Y.; Du, M.; Khan, A.; Usman, R.; Zhang, W.; Shan, H.; Xu, C. Tuning the Solid-State Fluorescence of Chalcone Crystals via Molecular Coplanarity and J-Aggregate. *RSC Adv.* **2017**, *7*, 8491–8503. [[CrossRef](#)]
43. Almeida, L.R.; Anjos, M.M.; Ribeiro, G.C.; Valverde, C.; Machado, D.F.S.; Oliveira, G.R.; Napolitano, H.B.; de Oliveira, H.C.B. Synthesis, structural characterization and computational study of a novel amino chalcone: A potential nonlinear optical material. *New J. Chem.* **2017**, *41*, 1744–1754. [[CrossRef](#)]
44. Kumar, C.S.C.; Loh, W.S.; Ooi, C.W.; Quah, C.K.; Fun, H.K. Heteroaryl chalcones: Design, synthesis, X-ray crystal structures and biological evaluation. *Molecules* **2013**, *18*, 12707–12724. [[CrossRef](#)] [[PubMed](#)]
45. Bakarić, D.; Baranović, G. The conformational equilibrium and vibrational properties of chalcone. *J. Mol. Struct.* **2019**, *1196*, 429–438. [[CrossRef](#)]
46. Spackman, P.R.; Turner, M.J.; Mckinnon, J.J.; Wolff, S.K.; Grimwood, D.J.; Jayatilaka, D.; Spackman, M.A. CrystalExplorer: A program for Hirshfeld surface analysis, visualization and quantitative analysis of molecular crystal. *J. Appl. Cryst.* **2021**, *54*, 1006–1011. [[CrossRef](#)] [[PubMed](#)]
47. Mackenzie, C.F.; Spackman, P.R.; Jayatilaka, D.; Spackman, M.A. CrystalExplorer Model Energies and Energy Frameworks: Extension to Metal Coordination Compounds, Organic Salts, Solvates and Open-Shell Systems. *IUCr* **2017**, *4*, 575–587. [[CrossRef](#)]
48. Spackman, M.A.; Jayatilaka, D. Hirshfeld surface analysis. *CrystEngComm* **2009**, *11*, 19–32. [[CrossRef](#)]
49. Tan, S.L.; Jotani, M.M.; Tiekink, E.R. Utilizing Hirshfeld surface calculations, non-covalent interaction (NCI) plots and the calculation of interaction energies in the analysis of molecular packing. *Acta Crystallogr. Sec. E Crystallog. Commun.* **2019**, *75*, 308–318. [[CrossRef](#)] [[PubMed](#)]
50. Parkin, A.; Barr, G.; Dong, W.; Gilmore, C.J.; Jayatilaka, D.; Mckinnon, J.J.; Spackman, M.A.; Wilson, C.C. Comparing entire crystal structure: Structural genetic fingerprint. *CrystEngComm* **2007**, *9*, 648–652. [[CrossRef](#)]

-
51. Spackman, M.A.; McKinnon, J.J. Fingerprinting intermolecular interactions in molecular crystals. *CrystEngComm* **2002**, *4*, 378–392. [[CrossRef](#)]
 52. Etter, M.C.; MacDonald, J.C.; Bernstein, J. Graph-Set Analysis of Hydrogen-Bond Patterns in Organic Crystals. *Acta Crystallogr. Sect. B Struct. Sci.* **1990**, *46*, 256–262. [[CrossRef](#)] [[PubMed](#)]
 53. Etter, M.C. Encoding and decoding hydrogen-bond patterns of organic compounds. *Acc. Chem. Res.* **1990**, *23*, 120–126. [[CrossRef](#)]
 54. McKinnon, J.J.; Jayatilaka, D.; Spackman, M.A. Towards Quantitative Analysis of Intermolecular Interactions with Hirshfeld Surfaces. *Chem. Commun.* **2007**, 3814–3816. [[CrossRef](#)] [[PubMed](#)]